Nano Energy 50 (2018) 756–765

Contents lists available at ScienceDirect

Nano Energy

journal homepage: www.elsevier.com/locate/nanoen

Full paper

Efficient and stable tandem luminescent solar concentrators based on carbon dots and perovskite quantum dots

Haiguang Zhao[a,b,*], Daniele Benetti[b], Xin Tong[b,c], Hui Zhang[b], Yufeng Zhou[b], Guiju Liu[a], Dongling Ma[b], Shuhui Sun[b], Zhiming M. Wang[c], Yiqian Wang[a,*], Federico Rosei[b,c,**]

[a] College of Physics & The State Key Laboratory, Qingdao University, No. 308 Ningxia Road, Qingdao 266071, PR China
[b] Centre Énergie Matériaux Télécommunications, Institut National de la Recherche Scientifique, 1650 Boulevard Lionel-Boulet, Varennes, Québec, Canada J3X 1S2
[c] Institute of Fundamental and Frontier Sciences, University of Electronic Science and Technology of China, Chengdu 610054, PR China

ARTICLE INFO

Keywords:
Quantum dots
Luminescent solar concentrator
Inorganic perovskite
Tandem
Carbon dots

ABSTRACT

Luminescent solar concentrator (LSC) can serve as large-area sunlight collectors, suitable for applications in building-integrated high-efficiency and low-cost photovoltaics. Inorganic perovskite quantum dots (QDs) are promising candidates as absorbers/emitters in LSCs, due to their high quantum yields (close to 100%), possibility of tuning size and chemical composition and broad absorption spectrum and high absorption coefficient. However, despite their great potential for technological development, LSCs fabricated using colloidal perovskite QDs still face major challenges such as low optical efficiency and limited long-term stability. Here we report a large-area (~ 100 cm^2) tandem LSC based on nearly reabsorption-free carbon dots (C-dots) and inorganic mixed-halide perovskite QDs spectrally-tuned for optimal solar-spectrum splitting. The as-fabricated semi-transparent device, without involving any complicated processes, exhibits an external optical efficiency of ~ 3% under sunlight illumination (100 mW/cm^2), which represents a 27% enhancement in efficiency over single layer LSCs based on $CsPb(Br_xI_{1-x})_3$ QDs and 117% over $CsPb(Cl_xBr_{1-x})_3$ QDs. Our work shows that the addition of C-dots can dramatically enhance the long-term durability of LSC devices based on perovskite QDs due to their excellent photostability and simultaneous absorption of ultraviolet light.

1. Introduction

Solar technologies, including photovoltaic (PV) devices and systems for hydrogen production, represent a promising opportunity to address the increasing demand for clean and renewable energy [1–4]. However, there are still several challenges that hinder the widespread deployment of these technologies, specifically: (a) low efficiencies of power conversion, (b) limited stability and (c) cost which is still too high to be competitive with other sources of energy. Overall, solar electricity generated by commercial PV devices is still considered comparatively expensive [5]. Luminescent solar concentrators (LSCs) can serve as low-cost large-area sunlight collectors for PV devices which could reduce the cost of electricity by decreasing the use of expensive PV materials and modules, also enhancing the power conversion efficiency (PCE) of PV devices thanks to the enhanced photon density incident onto the PV devices, which enhances their photocurrent [6–11].

A typical LSC consists of an optical waveguide (e.g. polymer or glass) embedded with highly emissive fluorophores [6–11]. Following the absorption of sunlight, the fluorophores re-emit photons, which are then guided by total internal reflection towards PV devices positioned at their edges, where they are converted into electricity by a solar cell (Fig. 1) [6–11]. LSCs can be made flexible and are low-cost, light-weight, and semi-transparent compared with commercial silicon or other PV panels [6–11]. LSCs may be used in building-integrated PV applications, such as transparent or semi-transparent solar roofs, solar facades, and space PV applications [12,13].

Compared with organic dyes/polymers [14,15], colloidal semiconductor nanocrystals (NCs) including inorganic quantum dots (QDs) such as core/shell PbS/CdS and CdSe/CdS QDs, inorganic perovskite NCs, carbon dots (C-dots), and doped quantum wells have recently emerged as more promising and efficient emitters in LSCs [7–13,16–19]. This is due to their high photoluminescence quantum yield (PL QY), size/chemical composition-tuneable broad absorption spectrum, narrow PL spectrum, high absorption coefficient and solution processability [7–13,16–19]. In addition, the overlap of their absorption and emission spectra can be engineered and minimized so as to

* Corresponding authors at: College of Physics & The State Key Laboratory, Qingdao University, No. 308 Ningxia Road, Qingdao 266071, PR China
** Corresponding author at: Centre Énergie Matériaux Télécommunications, Institut National de la Recherche Scientifique, 1650 Boulevard Lionel-Boulet, Varennes, Québec, Canada J3X 1S2
E-mail addresses: hgzhao@qdu.edu.cn (H. Zhao), yqwang@qdu.edu.cn (Y. Wang), rosei@emt.inrs.ca (F. Rosei).

https://doi.org/10.1016/j.nanoen.2018.06.025
Received 28 March 2018; Received in revised form 24 May 2018; Accepted 8 June 2018
2211-2855/ © 2018 Published by Elsevier Ltd.

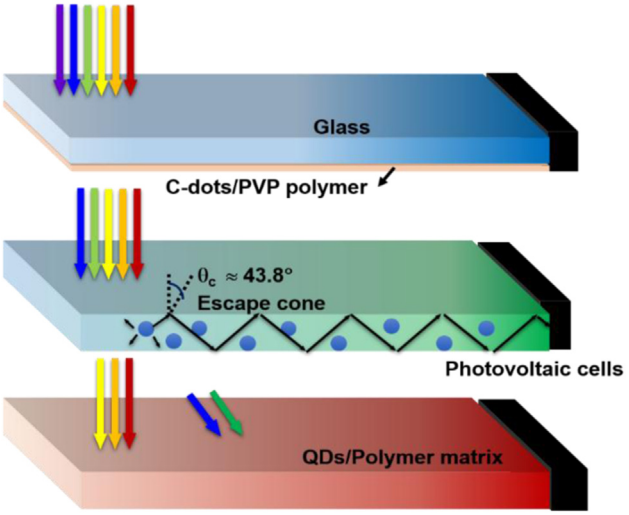

Fig. 1. C-dot and perovskite QDs based tandem LSCs. Scheme of a typical thin film LSC configuration with C-dots/polymer spin coated on a glass substrate (top). Scheme of mixed-halide perovskite $CsPb(Br_{1-x}Cl_x)_3$ QDs (middle) and $CsPb(Br_xI_{1-x})_3$ QDs (bottom) based LSCs by incorporating QDs into a polymer matrix.

suppress the energy loss caused by reabsorption [7–13,16–18]. Colloidal organic-inorganic and inorganic perovskite NCs have been synthesized [9,20–24] and were used as emitters for LSCs applications [9,23,24] in view of their high brightness with a PL QY up to 100% [25]. LSCs based on mixed-halide inorganic perovskite $CsPb(I_xBr_{1-x})_3$ QDs exhibit an external optical efficiency (defined as the ratio between the optical power of re-emitted photons reaching the edges of an LSC and the optical power of incident photons, also named PCE) of 2% with a lateral size of 1.3 × 7 cm^2 [9]. However, despite their great potential for technological development, LSCs fabricated using colloidal perovskite QDs still face the following major challenges: 1) the obtained external optical efficiency is still low compared with LSCs based on inorganic QDs (such as CuInSeS/ZnS and Si) [12,26]; ii) long-term stability of LSCs based on perovskite QDs is still limited by the stability of the perovskite materials themselves, due to their high sensitivity to moisture and ultraviolet (UV) light [20–24].

Current research efforts focus on improving the performance of LSCs by solving key challenges related to several types of energy loss: 1) a fraction of the absorbed light is re-emitted due to the non-unity PL QY of emitters; 2) reabsorption caused by the overlap between the absorption and emission spectra of the fluorophores; 3) the escaped emitted light as the refractive index of the polymer (or glass) is typically less than 1.5 (~ 75% of the emitted light trapped in an LSC waveguide), with the remainder ~ 25% lost from the top or bottom escape cone defined by Snell's Law (Fig. 1) [8,12,13]. Thus, the key requisite in terms of optical properties of fluorophores in high efficiency large-area LSCs includes high PL QY, minimal absorption and emission spectral overlap and broad absorption with significant overlap with the solar spectrum. Besides the energy loss in LSCs, the long-term stability of LSCs is still an open issue. The emitters used for LSCs easily degrade when exposed to environmental conditions, such as high humidity, UV light and high temperature (up to 100 °C) *etc* [7,13].

Several types of QDs were used as emitters to enhance the external optical efficiency of LSCs by improving their PL QY and engineering their Stokes shift (defined as the difference between the band maxima of absorption and emission spectra) [7,10,11,13,26]. For example, colloidal inorganic QDs including CdSe/CdS [13], CdSe/CdPbS [11], CdSe/CdZnS [7], CuInSeS/ZnS [12], PbS/CdS [10] and Si [26] exhibit a large Stokes shift in the 200–800 meV range and high PL QY in the range of 40–70%, leading to a conversion efficiency per incident photon of 1% in LSCs based on CdSe/CdS QDs (LSC dimensions: 21.5 × 1.3 × 0.5 cm^3) [13], 1.15% in LSCs based on CdSe/CdPbS QDs (LSC dimensions: 9 × 1.3 × 0.2 cm^3) [11] and 2.8% in LSCs based on Si QDs [26] (LSC dimensions: 12 × 12 × 0.26 cm^3). The currently reported record efficiency [3.2% in QDs [12] based LSC (12 × 12 × 0.2 cm^3) and 7.1% in dye [27] based LSC (5 × 5 × 0.5 cm^3)] is still well below the theoretical efficiency limit (21%) of LSCs as well as the target efficiency threshold for commercial products (10%) (Table 1) [28].

Table 1
Optical performance of reported LSCs based on QDs, C-dots and dyes.

Type of luminophore	Luminophore	LSC size (cm^3)	External optical efficiency	Ref.
QDs	CdSe/CdS	21.5 × 1.35 × 0.5	0.60%	[13]
QDs	$CuInSe_xS_{2-x}$/ZnS	12 × 12 × 0.3	3.20%	[12]
QDs	Silicon	12 × 12 × 0.26	2.85%	[26]
QDs	$CdSe/Cd_{1-x}Zn_xS$	90 × 30 × 0.16	–	[7]
QDs	$CdSe/Cd_xPb_{1-x}S$	7 × 1.5 × 0.3	1.40%	[11]
QDs	PbS/CdS	10 × 1.5 × 0.2	1.00%	[10]
QDs	Carbon Dots	2.5 × 1.6 × 0.1	4.75%	[19]
QDs (tandem)	$Mn:Cd_xZn_{1-x}S$/ ZnS + $CuInSe_2$/ ZnS	15.2 × 15.2 × 0.16	3.1%	[31]
Perovskite thin film	$CH_3NH_3PbI_3$	1.5 × 1.5 × 0.01	13.00%	[23]
Perovskite QDs	$CsPb(I_xBr_{1-x})_3$	9 × 1.3 × 0.2	2.00%	[9]
Dye (tandem)	BA241 + BA856	2 × 2 × 0.3	6.70%	[35]
Dye (tandem)	DCJTB + Pt (TPBP)	2.5 × 2.5 × 0.2	6.80%	[15]
Dye (tandem)	Lumogen F Red305 Fluorescence Yellow CRS040	5 × 5 × 0.5	7.10%	[27]
C-dots and perovskite QDs (tandem)	Carbon dots $CsPb(I_xBr_{1-x})_3$ $CsPb(Cl_xBr_{1-x})_3$	10 × 10 × 0.2	3.05%	This work

In addition to enhancing the PL QY and increasing the Stokes shift of QDs, a tandem structured LSC was demonstrated theoretically [29] and experimentally [15,27], improving the light absorption efficiency and decreasing the energy loss due to the light emitted because of the escape cone (Fig. 1). As already shown in the case of multiple-junction solar cells [30], or tandem LSCs based on dyes [15], absorbing different portions of the solar spectrum using different layers of emitters allows to realize high efficiency multi-layered LSCs compared with standard single-layer LSCs. For instance, dye based tandem thin film LSCs exhibit a PCE of 7.1% (with a diffusive back reflector) [27], which represents the highest reported for LSCs so far. However, the overall areas of tandem LSCs based on dyes are quite small, typically less than 25 cm^2, which is not suitable for the practical implementation of this technology [15,27]. To the best of our knowledge, there are until now only two reports for tandem LSCs using colloidal QDs [17,31]. Although inorganic perovskite QDs [9] and C-dots [19] have been separately used as emitters for single-layer LSC, there is still no report for fabricating tandem LSC by using a combination of perovskite QDs with C-dots. The rationale of combining them is that the C-dots will improve photostability of the perovskite-LSC because C-dots have a very good photostability under UV light.

Here we demonstrate the simultaneous use of C-dots with large Stokes shift and mixed-halide inorganic perovskite QDs as highly emissive fluorophores in high performance large-area (~ 100 cm^2) tandem LSCs. Specifically, we initially synthesized C-dots absorbing sunlight in the UV region via a hydrothermal approach (details included in the experimental section). The C-dots dispersed in methanol or water were subsequently mixed with polyvinylpyrrolidone (PVP) and spin-coated on a glass substrate. Then we synthesized mixed-halide $CsPb(Br_{1-x}Cl_x)_3$ and $CsPb(Br_xI_{1-x})_3$ perovskite QDs via a hot-injection approach and incorporated them into poly (lauryl methacrylate-*co*-ethylene glycol dimethacrylate) (PLMA-*co*-EGDA) polymer matrix, resulting in a semi-transparent composite. The as-fabricated semi-transparent tandem LSC based on C-dots and mixed-halide perovskite

QDs exhibits an external optical efficiency of ~ 3.05% under one Sun illumination. This represents a 27% and 117% enhancement in efficiency over single layer LSCs fabricated under the same conditions yet solely based on $CsPb(Br_xI_{1-x})_3$ QDs and $CsPb(Br_xCl_{1-x})_3$ QDs (LSC dimensions: $10 \times 10 \times 0.2\,cm^3$), respectively. More importantly, we found that the presence of C-dots can dramatically enhance the long-term photostability of LSC devices.

2. Results and discussion

2.1. Synthesis and structure of C-dots and perovskite QDs

C-dots were prepared via a hydrothermal approach, using citric acid and ethylenediamine or tris(hydroxymethyl)methyl aminomethane (Tris) as precursors dissolved in water (details reported in the experimental section, Table S1) [32,33]. C-dots were synthesized by using citric acid and ethylenediamine as precursors (defined as C-dots#1) and synthesized by using citric acid and Tris as precursors (defined as C-dots#2). The as-synthesized water-soluble C-dots (#1 or #2) exhibit a typical QY of 50% which is consistent with values reported in the literature [32,33]. For one batch of hydrothermal reaction (10 mL), the reaction yield reaches 50%, which produces 0.8 g of C-dots using citric and Tris as precursors. After purification, 0.5 g of C-dots are obtained from a one-batch reaction. X-ray photoelectron spectroscopy (XPS) measurements indicate that the samples consist of the same elements (C, N and O) in both C-dots#1 and C-dots#2 (Fig. S1). The atomic ratio of oxygen/nitrogen/carbon is 22.7/62.5/14.8 and 46.1/51.9/2 in C-dots#1 and C-dots#2, respectively (Table S2). The XPS results clearly demonstrate that the as-prepared C-dots#1 are capped with $–NH_2$, –OH and COOH groups, while in the case of C-dots#2 synthesized by Tris, they are mainly capped with hydroxyl groups ($–CH_2OH$) [32]. Transmission electron microscopy (TEM) was used to characterize the size of C-dots. As shown in Fig. 2a, the as-synthesized C-dots have an average diameter of ~ 2 nm.

In addition, colloidal inorganic perovskite QDs were synthesized via a hot injection method according to procedures reported in the literature [9]. By simply changing the molar ratio of $PbBr_2/PbCl_2$ salts, mixed-halide perovskites of $CsPb(Br_xCl_{1-x})_3$ can be readily synthesized (details provided in the experimental section). TEM was used to characterize the size and morphology of as-synthesized perovskite $CsPb(Br_xCl_{1-x})_3$ QDs (Fig. 2b). As shown in Fig. 2b, $CsPb(Br_{0.8}Cl_{0.2})_3$ mixed-halide QDs exhibit a typical cubic/cuboidal shape with edge dimension in the range 11–14 nm, similar with as-obtained and $CsPb(Br_{0.2}I_{0.8})_3$ QDs (Fig. 2c). The inset in Fig. 2c displays a high-resolution TEM (HRTEM) image of an individual $CsPb(Br_{0.2}I_{0.8})_3$ quantum dot (QD) with a lattice spacing of ~ 0.433 nm that is well indexed to the (110) plane of the cubic phase, consistent with selected-area electron diffraction (SAED) patterns of perovskite QDs (Fig. S3) [9]. The corresponding energy-dispersive x-ray spectroscopy (EDS) spectrum of $CsPb(Br_{0.2}I_{0.8})_3$ confirms the presence of Cs, Pb, and Br/I with an atomic ratio of 1:1:3 for $CsPb(Br_xI_{1-x})_3$ (Fig. S4). Similarly, the EDS spectrum of $CsPb(Br_xCl_{1-x})_3$ indicates that the molar ratio of Br/Cl is 4/1.

2.2. Optical properties of LSCs based on C-dots and perovskite QDs

We fabricated thin-film C-dot based LSCs by dispersing hydrophilic C-dots in methanol mixed with PVP and spin-coating them on a glass substrate with a lateral size of $10 \times 10\,cm^2$ (scheme displayed in Fig. 1). Compared with LSCs based on all polymer waveguides, the energy losses of thin film LSCs due to self-absorption and scattering at imperfections within the waveguide can be largely eliminated as the commercial optical glass has usually less imperfections compared with QDs/polymer matrix. The absorption and photoluminescence (PL) spectra of C-dots based LSCs are shown in Figs. 3a and S5. The absorption spectrum acquired from C-dots can be tuned over the UV wavelength range (300–400 nm). There is no significant difference with respect to absorption/PL spectra of C-dots by using different types of precursors (Figs. 3a and S5). A typical Stokes shift in the range of 650–730 meV was achieved for as-synthesized C-dots, indicating very small overlap between absorption and emission spectra (Fig. S5). A large Stokes shift in the as-synthesized C-dots indicates that the emission originates from the surface states, rather than the bandgap (or close bandgap) emission [33,34]. In addition, as-synthesized C-dots exhibit an excitation-wavelength independent emission spectrum, similar to the typical behaviour of inorganic QDs [12,13]. More importantly, the PL spectrum of as-synthesized C-dots ranging from 400 to 550 nm strongly overlaps with the absorption spectrum of mixed-halide perovskite QDs (Figs. 3 and S6). The emitted light from the C-dot layer due to the escape cone can be reabsorbed by the second layer of LSCs based on mixed-halide perovskite QDs, thereby improving the overall external optical efficiency of the device [17].

The second and third layers of tandem LSCs were fabricated by using mixed-halide perovskite QDs as emitters and further incorporated them into a PLMA polymer matrix (Fig. 3b and c) following the procedure reported in Ref. [9]. The typical absorption and emission spectra of $CsPb(Br_{0.8}Cl_{0.2})_3$ QDs were shown in Fig. 4. The as-synthesized $CsPb(Br_{0.8}Cl_{0.2})_3$ QDs have a typical PL QY of 70 ± 10% with a 2.5-fold larger Stokes shift (170 vs 70 meV) compared with $CsPbBr_3$ QDs. As reported previously [9], tuning the chemical composition of perovskite QDs by using mixed-halide precursors can enhance the Stokes shift due to their lower size uniformity [9]. The as-synthesized $CsPb(Br_{0.2}I_{0.8})_3$ QDs have a typical PL QY of ~ 60 ± 8%. The lateral size of LSCs based on mixed-halide perovskite QDs is $10 \times 10\,cm^2$.

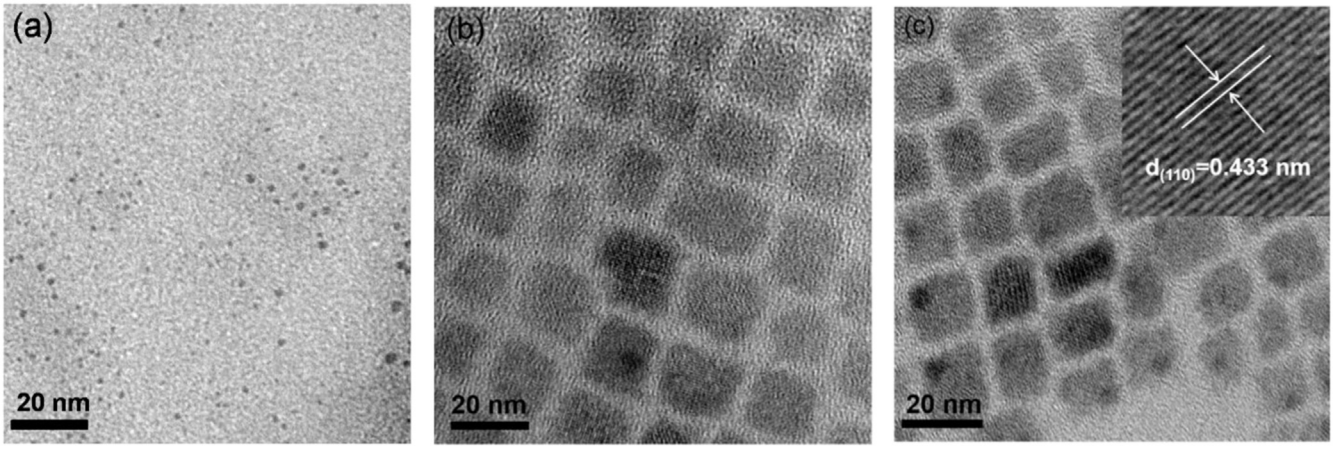

Fig. 2. Microstructure of C-dots and perovskite QDs. Representative TEM images of (a) C-dots#1, (b) $CsPb(Br_{0.8}Cl_{0.2})_3$ QDs and (c) $CsPb(Br_{0.2}I_{0.8})_3$ QDs. Inset of (c) shows typical HRTEM image of an individual perovskite QD.

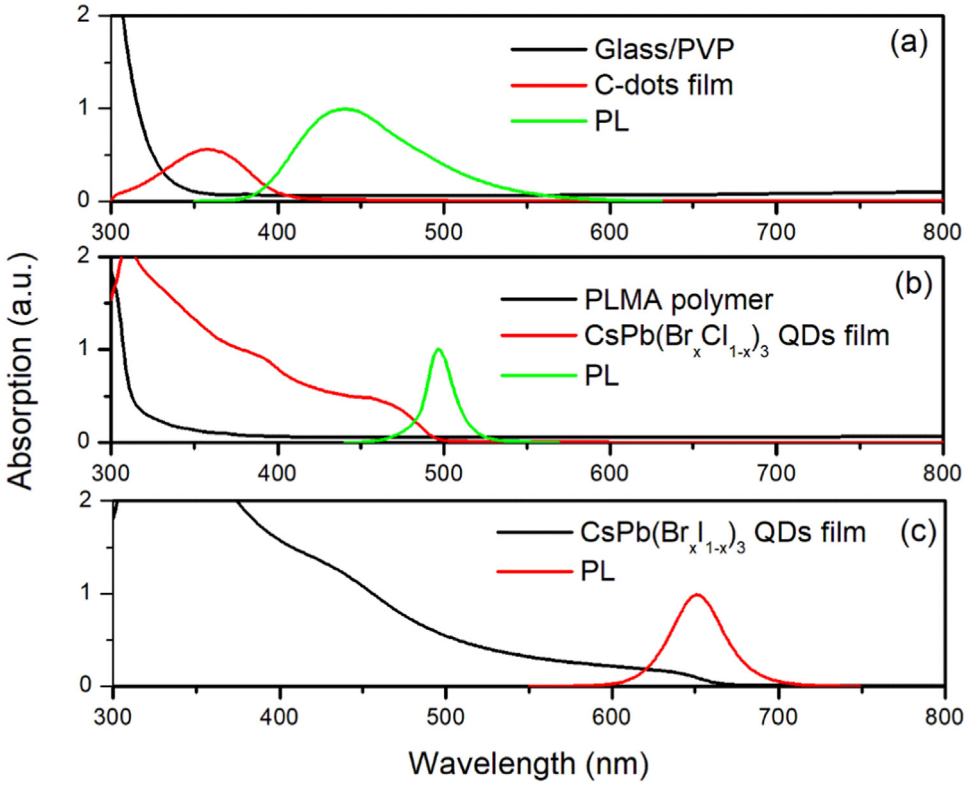

Fig. 3. Optical properties of LSCs based on QDs. Absorption and normalized PL spectra of LSCs based on C-dots/PVP on a glass substrate (a), $CsPb(Br_{0.8}Cl_{0.2})_3$ QDs (b) and $CsPb(Br_{0.2}I_{0.8})_3$ QDs (c) incorporated into a PLMA polymer matrix. The excitation wavelength is λ_{ex} = 350 nm for C-dots and λ_{ex} = 444 nm for perovskite QDs.

Before and after transferring the QDs from solution phase into PVP or PLMA polymer, there is no significant change in the PL QY for the investigated samples, as confirmed by PL decay measurements. Specifically, we estimated the relative PL QY of QDs in the polymer matrix (PVP or PLMA) by considering variations in lifetime [7,9,12,13].

The PL QY can be expressed as:

$$\text{PL QY} = \frac{k_{et}}{k_{et} + k_{net}}$$

where k_{et} and k_{net} are the radiative and non-radiative decay rates, respectively.

The measured PL lifetime is equal to:

$$\tau = \frac{1}{k_{et} + k_{net}}$$

The absence of additional non-radiative decay channels (k_{net}) in the C-dots and mixed-halide $CsPb(Br_{0.8}I_{0.2})_3$ and $CsPb(Br_{0.8}Cl_{0.2})_3$ QDs/polymer was confirmed by PL decay measurements, which show identical dynamics for the QDs before and after encapsulation in the polymer (Fig. 4). This result indicates that the synthetic process does not lead to the formation of a significant density of surface-defects/traps [12,13]. As reported in the literature, the LSC preparation process only affects the k_{net} of QDs [13]. Since

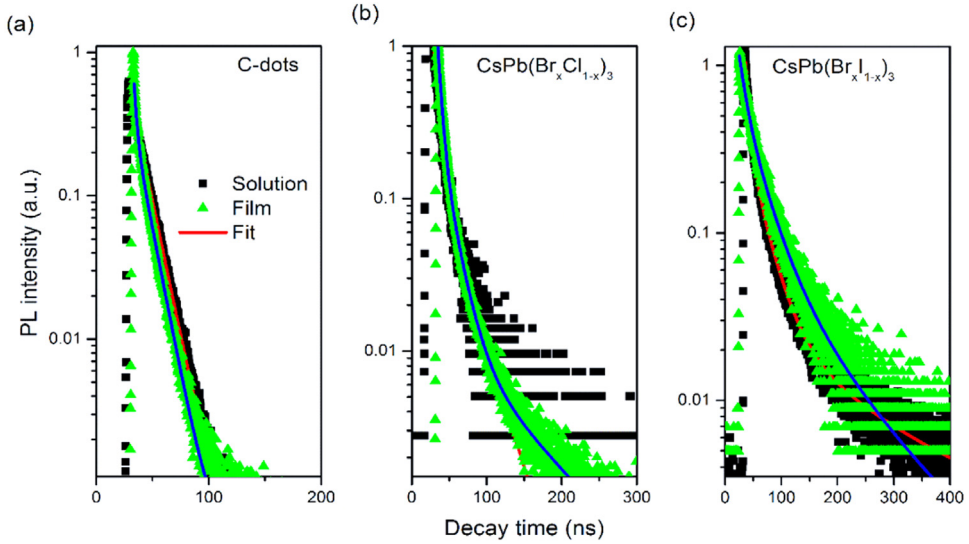

Fig. 4. PL decay in LSCs. (a) The PL decay curves of QDs in toluene and after embedding in polymer. (a) C-dots, (b) $CsPb(Br_{0.8}Cl_{0.2})_3$ QDs and (c) $CsPb(Br_{0.2}I_{0.8})_3$ QDs. The excitation wavelength is λ_{ex} = 350 nm for C-dots and λ_{ex} = 444 nm for perovskite QDs.

the measured PL lifetime of investigated C-dots or perovskite QDs does not change after embedding them in the polymer, we can deduce that the factor (k_{et} + k_{net}) does not change either [13]. This is a clear indication that both the C-dots and the mixed-halide QDs embedded in the polymer maintain a similar PL QY as those dispersed in solution.

As shown in Fig. 5a–c, LSCs based on C-dots and perovskite QDs exhibit very good transparency in the visible range, which is highly favourable for the development of solar windows. The estimated sunlight absorptances (η_{abs}, see experimental section for details) for the three LSCs are: 1.5%, 6.1% and 7.1% for the C-dots, $CsPb(Br_{0.8}Cl_{0.2})_3$ and $CsPb(Br_{0.2}I_{0.8})_3$, respectively. As shown in Fig. 5a–f, the large-area square LSC (0.2 × 10 × 10 cm^3) appears semi-transparent in ambient environment, and a clear concentrated light can be seen from the edges, when the top surface of the LSC is placed under one Sun illumination (100 mW/cm^2). Fig. 5 presents photographs of single-layer of LSC and three overlapping LSCs using C-dots (blue), $CsPb(Br_{0.8}Cl_{0.2})_3$ (green) and $CsPb(Br_{0.2}I_{0.8})_3$ (red) QDs under one Sun illumination, in which all blue, green and red emissions are clearly visible, indicating the successful fabrication of tandem semi-transparent LSCs using C-dots and mixed-halide perovskite QDs.

2.3. External optical efficiency in LSCs

For a quantitative investigation of the performance of LSCs, in the case of LSCs based on C-dots, we used square-shaped glass with thickness (D) of 2 mm and side length (L) of 10 cm, and for perovskite QDs based LSCs, we used a square-shaped PLMA polymer waveguide with D = 1.8 mm and L = 10 cm. The thickness (d) of the C-dots/PVP polymer layer is 100 μm. The geometrical gain factor (the ratio of the area of the top of the LSC and the area of the edges of the LSC coupled with the PV cells) is 14 in the case of LSC based on C-dots and 12 for LSCs based on perovskite QDs. These LSCs were illuminated perpendicularly to their surface by an AM 1.5G solar simulator (100 mW/cm^2). An optical power meter (or silicon PV) was coupled with one of the edges of the LSC and was used to measure the emitted light intensity. No significant difference can be found in the external optical efficiencies measured by silicon PV or optical power meter [9]. The single-layer LSC based on C-dots shows an external optical efficiency of 0.3% (Table 2). The LSCs based on $CsPb(Br_{0.8}Cl_{0.2})_3$ and $CsPb(Br_{0.2}I_{0.8})_3$ exhibit external optical efficiencies of 1.4% and 2.4%, respectively (Table 2). In the tandem LSC based on C-dots and perovskite QDs, the first layer LSC based on C-dots displays an external optical efficiency of 0.3%. The second layer of LSCs based on $CsPb(Br_{0.8}Cl_{0.2})_3$ QDs has an external optical efficiency of 1.1% and the third layer LSC based on $CsPb(Br_{0.2}I_{0.8})_3$ exhibits an external optical efficiency of 1.65%, resulting in an overall external optical efficiency of 3.05% (Table 2). The latter value (LSC dimension: 100 cm^2) is comparable with the best external optical efficiency (or PCE) reported in the literature (Table 1), such as 2.85% efficiency in single layer LSCs based on Si QDs [26] (LSC dimension: 144 cm^2), 3.2% efficiency in single layer LSCs based on $CuInSe_xS_{2-x}$/ZnS QDs [12] (LSC dimension: 144 cm^2), and 3.1% efficiency in tandem LSCs based on Mn:$Cd_xZn_{1-x}S$/ZnS and $CuInSe_2$/ZnS QDs [31] (LSC dimension: 230 cm^2). The obtained external optical efficiency is 3.05%, which is still lower than the value achieved in tandem LSCs based on dyes (for instance 7.1% [27], 6.8% [15] and 6.7% [35]). However, the area of tandem LSCs based on dyes is quite small, around 4–25 cm^2 [15,27,35], which are at least four-times smaller than that of tandem LSCs based on QDs (Table 1). The obtained efficiency is 1.5 times higher than that of the singe-layer LSC based on $CsPb(Br_xI_{1-x})_3$ QDs reported previously (LSC dimension: 12 cm^2) [9].

Table 2
External optical efficiencies for single-layer and tandem LSCs based on different types of QDs under one Sun illumination (100 mW/cm^2).

LSCs		External optical efficiency (%)	
C-dots#1		0.35 ± 0.05	
C-dots#2		0.3 ± 0.05	
$CsPb(Br_{0.8}Cl_{0.2})_3$ QDs		1.4 ± 0.1	
$CsPb(Br_{0.2}I_{0.8})_3$ QDs		2.4 ± 0.2	
Tandem LSCs	C-dots#2	0.3 ± 0.05	3.05 ± 0.2
	$CsPb(Br_{0.8}Cl_{0.2})_3$ QDs	1.1 ± 0.1	
	$CsPb(Br_{0.2}I_{0.8})_3$ QDs	1.65 ± 0.15	

The enhancement in the external optical efficiency in the tandem LSC over single-layer LSC is attributed to the following effects: i) tandem structures have much stronger overall absorption across the solar spectrum compared with a single layer LSC [17,31]; ii) the escaped emitted light due to the escape cone can be reabsorbed by the bottom layer of LSC; iii) the reabsorption energy loss in LSCs based on perovskite QDs due to the spectral overlap of absorption and emission could be mitigated by blocking high energy UV light by using the C-dots layer [17]. Using an analytical model of planar LSCs, which was confirmed to be accurate by comparing it with Monte Carlo ray-tracing simulations [7], we can predict the efficiency of large-area LSCs and also simulate the variation of different parameters, such as the PL QY of the QDs (or C-dots) on the external optical efficiency of LSCs.

As shown in Fig. 6, the analytical model, using values of PL QY close to the experimental ones, is a very good fit for the experimental points of the three separate LSCs and for the tandem system. In Fig. 6a we observe the effect of increasing the size of the three single LSC under full Sun exposure. Doubling the area (200 cm^2) while maintaining the same PL QY would

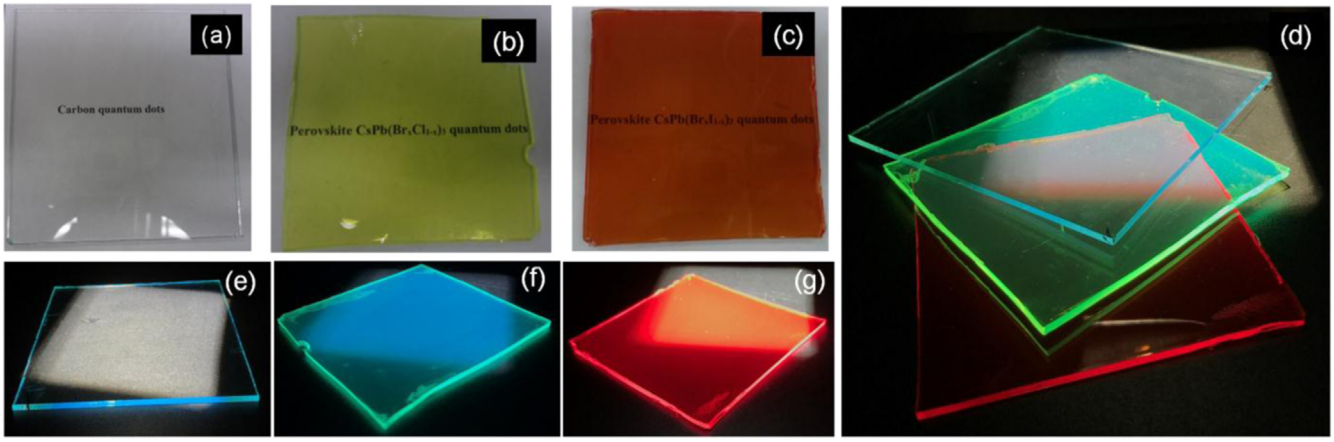

Fig. 5. Photographs of QD–polymer composites. Photographs of the LSC comprising C-dots under ambient (a) and under one Sun illumination (100 mW/cm^2) (e), $CsPb(Cl_{0.2}Br_{0.8})_3$ QDs under ambient (b) and one Sun illumination (f), and $CsPb(Br_{0.2}I_{0.8})_3$ QDs under ambient (c) and one Sun illumination (g). (d) LSCs based on QDs under one Sun illumination. LSC dimensions, 10 × 10 × 0.2 cm^3. The weight concentration of perovskite QDs in PLMA is 1.3% (calculated based on the Themogravimetric Analyzers (TGA), Fig. S7).

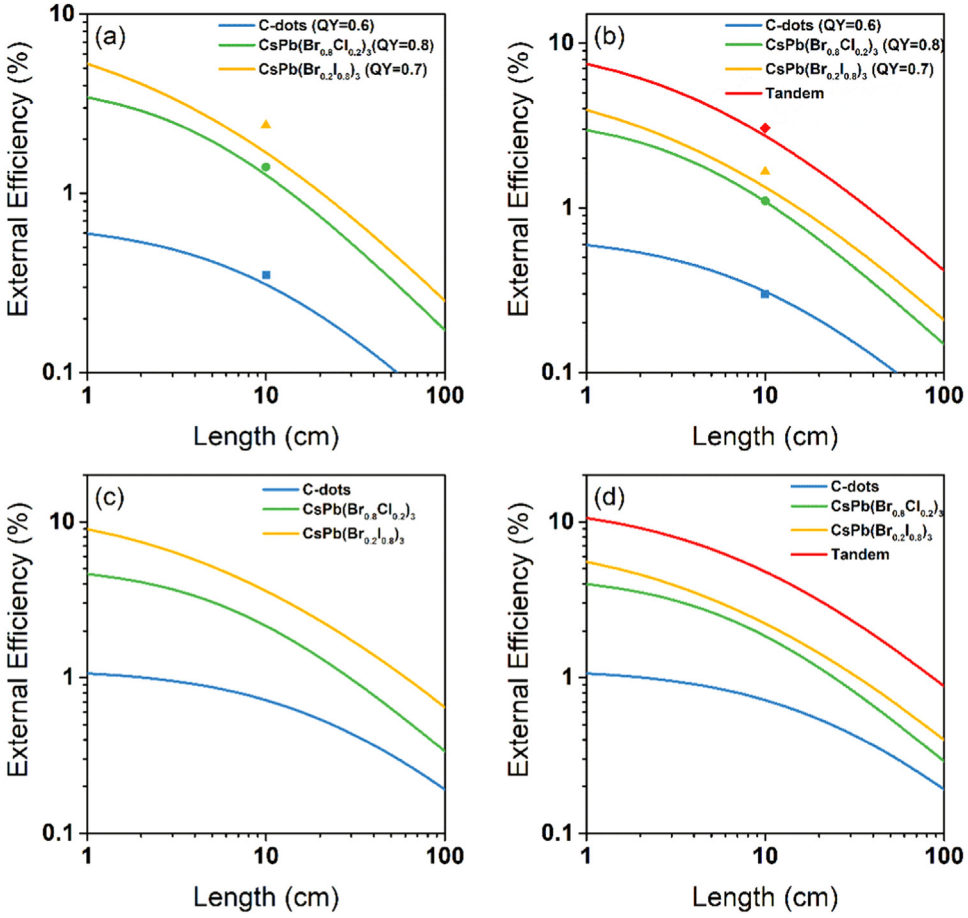

Fig. 6. Analytical model of the performance of the different LSCs. (a) External efficiency of the single LSC under one Sun illumination, with the experimental PL QY. The square points are the experimental data obtained with the power meter. (b) External efficiency of the tandem LSC solution (red line) and of the single LSC under spectrum filtered by the different layers (see experimental methods for details). External efficiencies for single LSCs (c) and tandem LSC (d) with ideal QY = 1.

produce efficiencies of 0.2%, 0.75% and 1% for C-dots, $CsPb(Br_{0.8}Cl_{0.2})_3$ and $CsPb(Br_{0.2}I_{0.8})_3$ LSCs, respectively. Fig. 6b clearly shows the beneficial effect of employing a tandem structure. The external optical efficiency for each of single LSC, as experimentally measured, is smaller compared with the case of LSC fully illuminated by one Sun, while the tandem structure always achieves higher efficiencies. Comparing again LSCs with area double the one we measured, we observed that the tandem LSC reaches an external optical efficiency of 1.7%. In Fig. 6c and d, we explored the case of ideal PL QY, i.e. 100%, for all the three emitters. As expected all the external optical efficiencies increase, and in particular the tandem structure with area double the one realized, would maintain the same efficiency (3.1%). We observe that the beneficial effect of the tandem structure is slightly reduced. The tandem solution still represents the best choice as it guarantees a much higher photostability (details in the next section). In Fig. S8, we reported the results of the variation of the PL QY for single LSCs under one Sun. In general for L = 10 cm (A = 100 cm^2), increasing the PL QY of the C-dots from 60% to 80% would increase the efficiency from 0.3% to 0.5%, while for the $CsPb(Br_{0.8}Cl_{0.2})_3$ an increase from 80% to 90% would increase the efficiency from 1.3% to 1.7%. Lastly, for $CsPb(Br_{0.2}I_{0.8})_3$, an increase of the PL QY to 90% would yield LSCs with efficiency of 2.7%.

We further measured the PL spectra of the C-dots or perovskite QDs based single layer LSC at different optical paths (Fig. S9) by using the optical set-up shown in Fig. S10. We plotted the integrated PL intensity as a function of the optical paths. As shown in Fig. S9, the integrated PL intensity of $CsPb(Br_{0.2}I_{0.8})_3$ and $CsPb(Br_{0.8}Cl_{0.2})_3$ decreases to 50% of its initial value in eight cm LSC, due to both emitted photons and re-absorption energy loss. In the case of C-dots, the integrated PL intensity remains 0.68 in an eight cm LSC (Fig. S9d). The smaller energy loss in single layer LSC based on C-dots compared with those based on perovskite QDs is due to both the lower reabsorption energy loss and fewer escaped emitted photons. During each reabsorption or scattering event, additional photons will be lost due to the escape cone. In the PLMA polymer based LSC, there are more defects which lead to more scattering compared with the thin film LSC based on C-dots, in which the high-quality glass endows the less scattering of emitted photons.

2.4. Stability in LSCs based on C-dots and mixed-halide perovskite QDs

In general, compared with core/shell QDs, such as PbS/CdS and CdSe/CdS QDs, perovskite QDs are more sensitive to humidity and UV light. We found that the PL signal of perovskite QDs is very sensitive to exposure to humidity of 30%. On the other hand, it is still possible to maintain their optical properties unaltered including their PL QY, PL peak positions and peak widths by embedding them in a polymer matrix for at least a year, due to the good isolation of QDs from oxygen or humidity. It was found that the PL intensity of LSCs based on perovskite $CsPb(Br_xI_{1-x})_3$ QDs maintains 90% of its initial value after ten hours illumination (400 nm light emitting device with an intensity of 200 mW/cm^2) [9]. Klimov's group found that 91% of the original PL QY of LSCs based on silica coated core/shell $CdSe/Cd_{0.6}Zn_{0.4}S$ QDs is preserved after 200 h illumination (462 nm light emitting device with an intensity of 1.57 W/cm^2) under N_2 atmosphere (H_2O and O_2 below 1 ppm) in a glove box [17]. These results indicate that LSCs based on core/shell QDs exhibit better photostability than LSCs based on perovskite QDs. The issue of long-term photostability in perovskite QDs limits their potential application as bright emitters for LSCs. The PL intensity of LSCs based on inorganic mixed-halide perovskite gradually decreases upon exposure to a high dose of UV illumination (365 nm light emitting device with an intensity of 200 mW/cm^2) under ambient conditions (40% humidity at 25 °C) without an LSC based on C-dots#2 (Fig. S11). As shown in Fig. 7b, only ~ 50% of the integrated PL intensity of LSCs based on mixed-halide $CsPb(Br_{0.2}I_{0.8})_3$ and $CsPb(Br_{0.8}Cl_{0.2})_3$ perovskite QDs was maintained after 70-h illumination. In stark contrast, with the presence of LSCs based on C-dots (#1 or #2), there is

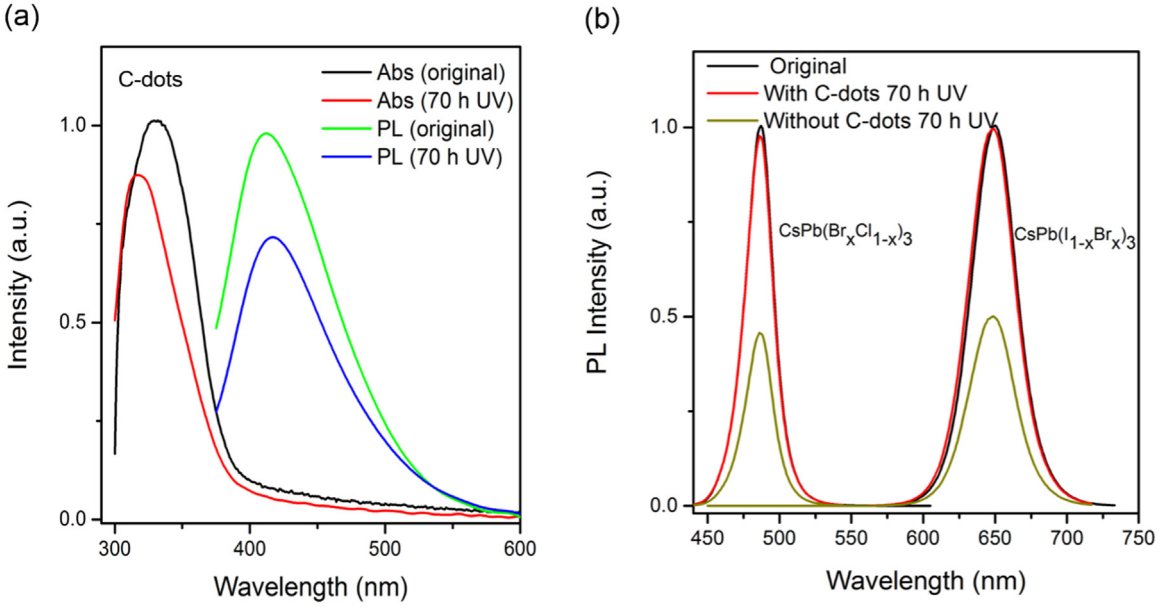

Fig. 7. Stability of LSCs based on different types of QDs. (a) Absorption and PL spectra of C-dots #2 based LSCs. (b) PL spectra of $CsPb(Br_{0.8}Cl_{0.2})_3$ and $CsPb(Br_{0.2}I_{0.8})_3$ QDs based LSCs. All LSCs were illuminated upon UV exposure for 70 h under ambient conditions. For the LSCs based on perovskite QDs, the stability was tested by placing the LSCs directly under UV light or placing the LSC under the LSC based on C-dots on a glass substrate.

no significant variation in PL intensity of LSCs based on perovskite QDs (Figs. 7b and S11). Inorganic perovskites typically exhibit much higher photostability compared to organic-inorganic hybrid perovskites. Significant variations in the PL FWHM and PL peak position are generally attributed to a phase segregation which creates iodide-rich and bromide-rich domains in mixed halide perovskite QDs [36]. In our case, the PL widths and PL peak position do not show any significant change, indicating there is no phase segregation. To understand the decrease of PL intensity for the LSC based on perovskite QDs, we further calculated the absorbed power by the first-layer LSC based on C-dots. The optical density of the C-dots film at the excitation wavelength (365 nm) was 0.57 (0.07 of PVP/glass), indicating that the absorbed power was 146 mW/cm^2 [7]. Thus the UV power is only 54 mW/cm^2 on the second layer of LSC based on $CsPb(Br_{0.8}Cl_{0.2})_3$ QDs. Similarly, the optical density of the $CsPb(Br_{0.8}Cl_{0.2})_3$ film at the excitation wavelength (365 nm) was 1.3, indicating that the absorbed power was 51 mW/cm^2 [7]. Thus the UV power is only 3 mW/cm^2 on the second-layer of LSC based on $CsPb(Br_{0.8}Cl_{0.2})_3$ QDs. We also calculated the total photon flux of the sunlight passing after the first layer (after C-dots absorption) and after passing through the second layer. As shown in Fig. S12, the UV flux impinging on the second layer is strongly reduced (51% of the original flux between 300 nm and 400 nm) and almost zero on the third layer (4%).

We further investigated the photostability of LSCs based on mixed-halide perovskite QDs under low UV dose (20 mW/cm^2). We did not observe any significant PL variation after 70-h illumination, which confirms that the low UV-light intensity is the main reason for the improved PL photostability of LSCs based on perovskite QDs. As shown in Fig. 7a, the integrated PL intensity in LSCs based on C-dots#2 still maintains 77% of its initial value, which is much higher than that (48%) in LSC based on C-dots#1 (Fig. S13). The blue shift in the first-excitonic absorption peak in C-dots#2 is attributed to UV-induced photo-bleaching [30]. The superior photostability of the C-dots#2 compared with C-dots#1 is mainly ascribed to its surface being capped with the hydroxyl groups (–CH_2OH) as confirmed by XPS spectra (Fig. S1) [33]. A cone-like shape on the C-dots#2 outer surface was obtained through chemical bonding due to the steric crowding effect of the dendritic hydroxyl methyl groups which can effectively slow down the diffusion of oxygen into the fluorescence centers, protecting the C-dots from degradation induced by photo-oxidation [33].

We further estimate the cost and cost/power ratio of C-dots or inorganic perovskite QDs (details in SI, Tables 3 and S3–4). The cost of C-dots ($/g) is at least 40 times cheaper than the cost of perovskite QDs and the cost/power ratio of C-dots based LSC at least 20 times smaller than that of LSC based on perovskite QDs (Table 3). In addition, the synthesis procedure for C-dots is very simple. It is a reasonable strategy to use C-dots layer to improve the durability of LSCs based on perovskite QDs. In addition, there is no significant change in their external optical efficiency after storing at ambient conditions for more than six months. These results indicate that tandem LSCs based on combining inorganic perovskite QDs and C-dots are very promising for solar energy applications.

Future performance improvement of tandem LSC based on C-dots and perovskite QDs should focus on the following directions: i) improving the external optical efficiency by optimizing the structure and size of perovskite QDs to enhance their PL QY and Stokes shift [16,37,38]. For example, a larger Stokes shift can be obtained by synthesizing small-sized perovskite QDs or Mn-doped perovskite QDs [16], and a near 100% PL QY of perovskite QDs can be obtained directly or after post-treatment [37,38]. ii) enhancing the efficiency and photostability of LSCs by optimizing the performance of C-dots [39,40]. For instance, the PL QY of C-dots can be enhanced to 99% [40].

3. Conclusions and perspectives

In summary, we demonstrated high-efficiency and large-area tandem LSCs based on colloidal C-dots and mixed-halide perovskite

Table 3
Estimated cost/power ratio of LSC based on C-dots and perovskite QDs. The calculation only considers the cost of chemicals used for fabrication of LSC with 1 m^2 surface area (the thickness of LSC is around 1.8 mm). The weight percentage of perovskite QDs in PLMA is 1.3% and the weight percentage for C-dots is around 1.5%. The thickness of C-dots is around 100 μm. During spin-coating, for LSC with area of 100 cm^2, 4 mL of C-dots were used.

QDs	Price per 1 m^2 LSC	External optical efficiency	Cost/power ratio
C-dots#1	6$	0.35%	1.7$/mW
C-dots#2	4$	0.3%	1.3$/mW
$CsPb(Br_{0.8}Cl_{0.2})_3$	1300$	1.4%	93$/mW
$CsPb(Br_{0.2}I_{0.8})_3$	1000$	2.4%	42$/mW

QDs. All QDs exhibit a large Stoke shift and high PL QYs of 50–70%. The as-fabricated semi-transparent tandem LSCs exhibit an external optical efficiency of ~ 3.05% under sunlight illumination (100 mW/cm^2) which represents a 27% enhancement in efficiency compared with single layer LSCs based on $CsPb(Br_xI_{1-x})_3$ QDs and 117% over $CsPb(Br_xCl_{1-x})_3$ QDs (LSC dimension: 100 cm^2) because of the tandem geometry of LSCs based on different types of QDs with spectrally-tuned for optimal solar-spectrum splitting. More importantly, the presence of C-dots significantly enhances the long-term photostability of LSC devices based on perovskite QDs due to the excellent photostability of C-dots and its strong absorption for UV light, which decreases the UV intensity in the pervoskite QDs based LSC.

In view of the simple and low-cost synthetic procedure and excellent optical properties of C-dots and mixed-halide perovskite QDs, they represent an efficient emitter for low-cost, large-area and high efficiency tandem LSCs for both semi-transparent windows and sunlight collectors for PV devices. Using C-dots to enhance both the efficiency and photostability of LSCs can be applied to LSCs made of other types of QDs, such as CdSe/CdS QDs, PbS/CdS QDs and CuInSSe/ZnS QDs. Future work should focus on further improving the PL QY of C-dots in order to further improve the efficiency of tandem LSCs.

4. Methods

4.1. Chemicals and materials

Oleic acid (OA, 90%), citric acid, ethylenediamine, octadecene (ODE), oleylamine (OLA, > 98%), tris(hydroxymethyl)methyl aminomethane (Tris), Cs_2CO_3 (99%), butanol, lead(II) iodide (PbI_2, 99.999%), lead chloride ($PbCl_2$ 99.999%), methanol, lead(II) bromide ($PbBr_2$, 99.999%), Rhodamine 6 G, lauryl methacrylate, ethylene glycol dimethacrylate, (diphenyl(2,4,6-trimethylbenzoyl)phosphine oxide, PVP (MW: 40000), and toluene were purchased from Sigma-Aldrich. All chemicals were used as purchased.

4.2. Synthesis of C-dots

C-dots were prepared via a hydrothermal approach [32]. Typically, 0.42 g citric acid and 536 μL ethylenediamine were dissolved in 10 mL water under stirring. Subsequently the precursors were transferred into an autoclave and reacted for 6 h at 200 °C.

We also synthesized hydroxyl group functionalized C-dots using citric acid and Tris as precursors [33]. Typically, 1.051 g citric acid and Tris (0.6084 g) were dissolved in 10 mL water under stirring. Subsequently the precursors were transferred into an autoclave and reacted for 6 h at 200 °C.

The as-synthesized reaction solution (in water) was transferred into dialysis bags with molecular weight of 3000 Da. The dialysis bags were immersed in the methanol solution for two hours at room temperature. The C-dots methanol solution outside the dialysis bag was collected and concentrated into 15 mg/L by evaporating the methanol in nitrogen flow. Finally the as-obtained C-dots solution was kept in the refrigerator at − 10 °C.

4.3. Synthesis of Cs-oleate

A solution of OA (0.6 mL) and Cs_2CO_3 (0.2 g) in 7.5 mL of ODE was stirred and heated to 200 °C until the white powder was completely dissolved [9]. The mixture was subsequently kept at 130 °C for one hour under vacuum. The temperature of the Cs-oleate mixture was kept at least at 60 °C to avoid precipitation.

4.4. Synthesis of perovskite QDs

Perovskite QDs were synthesized by using a hot injection approach [9]. Typically, in a 100 mL round-bottom flask, OA (2 mL), OLA (2 mL), ODE (20 mL) and 290 mg of $PbBr_2$ were degassed at 100 °C for 30 min. The reaction flask was re-stored with N_2 and heated to 130 °C for 30 min under vacuum. The temperature was further increased to 160 °C, followed by rapid injection of 2 mL of Cs-oleate solution. The reaction was kept at 160 °C for five seconds, then the solution was rapidly cooled by the water bath. For the synthesis of the mixed-halide perovskite QDs, a mixture of $PbBr_2/PbI_2$ or $PbCl_2/PbBr_2$ with molar ratio 2:8 was used as halide precursors. All other reaction conditions, such as injection temperature and reaction time are the same with the synthesis of $CsPbBr_3$ QDs. Butanol was added, then the suspension was centrifuged and the supernatant was removed. The purification process was repeated twice. The QDs were then dispersed in toluene for further characterization. The as-prepared QDs are observed to be very sensitive to moisture and need to be kept in a desiccator or a refrigerator at − 10 °C.

4.5. LSCs based on C-dots/PVP thin film on a glass substrate

The C-dots dispersed in methanol were mixed with PVP polymer with a final concentration of PVP of 200 mg/mL. The concentration of C-dots is around 15 mg/mL. The mixture was then spin-coated on a glass substrate with a speed of 500 r.p.m. and an acceleration rate of 800 r.p.m. for one min with a thickness of 50–100 μm. The glass thickness is around 2 mm.

4.6. LSCs based on perovskite QDs/PLMA polymer

The LSCs were fabricated by embedding perovskite QDs in the polymer matrix. Perovskite QDs (50 mg) dispersed in toluene were added to a 50 mL flask and the solvent vapor was pumped away. The monomer precursors of lauryl methacrylate and ethylene glycol dimethacrylate (wt% of 5:1) and a UV initiator (diphenyl(2,4,6-trimethylbenzoyl)phosphine oxide were mixed and sonicated until a colourless solution (3 mL) was obtained. The solution was then transferred into the flask containing solvent free perovskite QDs. The mixture was homogeneously dispersed by ultrasound treatment, then injected into a mold consisting of two glass slides separated by a flexible silicon rubber spacer of thickness ~ 1.8 mm. The mixture was kept under UV illumination (with a wavelength of 400 nm) for 2 h.

4.7. Characterization

TEM characterization of the QDs was carried out using a JEOL JEM2100F TEM equipped with an EDS. TGA (Q500) was used to identify the concentration of QDs inside the LSCs. XPS data were obtained using a VG Escalab 220i-XL equipped with a twin Al source and subsequently analyzed using the Casa XPS software. Absorption spectra were acquired with a Cary 5000 UV–vis–NIR spectrophotometer (Varian) with a scan speed of 600 nm/min. Fluorescence spectra were acquired with a Fluorolog-3 system (Horiba Jobin Yvon Incorp.). The PL lifetime of the perovskite QDs in solution and in the polymer matrix was measured using a pulsed laser diode of 440 nm and Time-Correlated Single Photon Counting (TCSPC) mode in the Fluorolog-3 system. PL QYs of C-dots and QDs were measured by using Rhodamine 6G as a reference.

The PL intensity of LSCs based on different types of QDs (C-dots, mixed-halide perovskite QDs) was measured by PL spectroscopy upon UV illumination (365 nm light emitting device with an intensity of 200 mW/cm^2 measured using a power meter, Newport Model 843-R) in ambient conditions.

The external optical efficiency of the LSCs was measured by using an ABET2000 solar simulator at AM 1.5G (100 mW/cm^2) calibrated using a reference Si solar cell. The external optical efficiency was tested under illumination upon the top area of the LSC using an ABET2000 solar simulator at AM 1.5G (100 mW/cm^2), with one edge mounted with a power meter.

4.8. Analytical model for efficiency of LSC

Following the formalism developed elsewhere [41], the external

efficiency of the LSC can be expressed as:

$$\eta_{external} = \eta_{abs}\,\eta_{internal} \quad (1)$$

in which η_{abs} is the sunlight absorptance and $\eta_{internal}$ is the internal efficiency.

η_{abs} can be calculated as:

$$\eta_{abs} = (1-R)\frac{\int_0^\infty I_{in}(\lambda)\lambda(1-e^{-\alpha(\lambda)d})d\lambda}{\int_0^\infty I_{in}(\lambda)\lambda d\lambda}$$

In which α is the absorption coefficient (calculated as $\alpha = \ln(10)\frac{A}{d}$, where d is the length and A the absorption), I_{in} is the Sun irradiance and R is the fraction of the incident light reflected by the collecting surface, that can be calculated, considering the normal incidence of the simulated sunlight as follows:

$$R = \frac{(n_{polymer} - n_{air})^2}{(n_{polymer} + n_{air})^2}$$

In the case of the polymer we used, R can be estimated to be 3% (Ref. [23]).

Since our experimental data on optical efficiency have been obtained under a simulated solar light with non-monochromatic spectrum, we used a spectrally averaged internal efficiency over the PL emission of the QDs $S_{PL}(\lambda)$, calculated as:

$$\eta_{internal} = \frac{\int_0^\infty \frac{\eta_{PL}\eta_{TIR}}{1+\beta\alpha(\lambda)L(1-\eta_{PL}\eta_{TIR})}S_{PL}(\lambda)d\lambda}{\int_0^\infty S_{PL}(\lambda)d\lambda}$$

in which $S_{PL}(\lambda)$ is the PL emission spectrum, η_{PL} is the estimated QY of the QDs, η_{TIR} is the total internal reflection efficiency of the polymer waveguide that can be estimated to be around 75%; β is a numerical value fixed to 1.4 and L is the length of the LSC.

Acknowledgements

F.R. is grateful to the Canada Research Chairs program for funding and partial salary support and to NSERC for an individual Discovery Grant. F.R. also acknowledges a Changjiang scholar award (Government of China) and Sichuan province for a 1000 talents short term award. H. Zhang acknowledges his Ph.D. Excellence scholarship from the UNESCO Chair and FQRNT. Y.Q. Wang would like to thank financial support from the Top-notch Innovative Talent Program of Qingdao City (Grant No. 13-CX-8) and the Taishan Scholar Program of Shandong Province, China, the Qingdao International Center for Semiconductor Photoelectric Nanomaterials, and Shandong Provincial University Key Laboratory of Optoelectrical Material Physics and Devices. D. Ma acknowledges funding from the NSERC through the Discovery Grant program. H.G. Zhao acknowledges funding from Qingdao University and the Natural Science Foundation of Shandong Province (ZR2018MB001). Y.F. Zhou acknowledges her Ph.D. Excellence Scholarship from the UNESCO Chair.

Appendix A. Supplementary material

Supplementary data associated with this article can be found in the online version at http://dx.doi.org/10.1016/j.nanoen.2018.06.025.

References

[1] U. Bach, D. Lupo, P. Comte, J.E. Moser, F. Weissortel, J. Salbeck, H. Spreitzer, M. Gratzel, Nature 395 (1998) 583–585.
[2] G. Selopal, H. Zhao, D. Benetti, X. Tong, F. Navarro-Pardo, Y. Zhou, D. Barba, F. Vidal, Z. Wang, F. Rosei, Adv. Funct. Mater. 27 (2017) 1701468.
[3] H. Zhao, F. Rosei, Chem 3 (2017) 229–258.
[4] X. Tong, Y. Zhou, L. Jin, K. Basu, R. Adhikari, G.S. Selopal, X. Tong, H. Zhao, S. Sun, A. Vomiero, Z.M. Wang, F. Rosei, Nano Energy 31 (2016) 441–449.
[5] A. Louwen, W. Sark, R. Schropp, A. Faaij, Sol. Energy Mater. Sol. Cells 147 (2016) 295–314.
[6] M.G. Debije, P.P.C. Verbunt, Adv. Energy Mater. 2 (2012) 12–35.
[7] K. W, H. Li, J. Lim, H.J. Song, V.I. Klimov, Nat. Energy 1 (2016) 16157.
[8] I. Coropceanu, M.G. Bawendi, Nano Lett. 14 (2014) 4097–4101.
[9] H. Zhao, Y. Zhou, D. Benetti, D. Ma, F. Rosei, Nano Energy 37 (2017) 214–223.
[10] Y. Zhou, D. Benetti, Z. Fan, H. Zhao, D. Ma, A.O. Govorov, A. Vomiero, F. Rosei, Adv. Energy Mater. 6 (2016) 1501913.
[11] H. Zhao, D. Benetti, L. Jin, Y. Zhou, A. Vomiero, F. Rosei, Small 12 (2016) 5354–5365.
[12] F. Meinardi, H. McDaniel, F. Carulli, A. Colombo, K.A. Velizhanin, N.S. Makarov, R. Simonutti, V.I. Klimov, S. Brovelli, Nat. Nanotechnol. 10 (2015) 878–885.
[13] F. Meinardi, A. Colombo, K.A. Velizhanin, R. Simonutti, M. Lorenzon, L. Beverina, R. Viswanatha, V.I. Klimov, S. Brovelli, Nat. Photonics 8 (2014) 392–399.
[14] R. Rondao, A.R. Frias, S.F.H. Correia, L. Fu, V.Z. Bermudez, P.S. Andre, R.A.S. Ferreira, L.D. Carlos, ACS Appl. Mater. Interfaces 9 (2017) 12540–12546.
[15] M.J. Currie, J.K. Mapel, T.D. Heidel, S. Goffri, M.A. Baldo, Science 321 (2008) 226–228.
[16] F. Meinardi, Q.A. Akkerman, F. Bruni, S. Park, M. Mauri, Z. Dang, L. Manna, S. Brovelli, ACS Energy Lett. 2 (2017) 2368–2377.
[17] Y. Zhou, D. Benetti, X. Tong, L. Jin, Z.M. Wang, D. Ma, H. Zhao, F. Rosei, Nano Energy 44 (2018) 378–387.
[18] M. Sharma, K. Gungor, A. Yeltik, M. Olutas, B. Guzelturk, Y. Kelestemur, T. Erdem, S. Delikanli, J.R. McBride, H.V. Demir, Adv. Mater. 29 (2017) 1700821.
[19] Y. Li, P. Miao, W. Zhou, X. Gong, X. Zhao, J. Mater. Chem. A 5 (2017) 21452–21459.
[20] E. Yassitepe, Z.Y. Yang, O. Voznyy, Y. Kim, G. Walters, J.A. Castaeda, P. Kanjanaboos, M.J. Yuan, X.W. Gong, F.J. Fan, J. Pan, S. Hoogland, R. Comin, O.M. Bakr, L.A. Padilha, A.F. Nogueira, E.H. Sargent, Adv. Funct. Mater. 26 (2016) 8757–8763.
[21] X. Chen, L.C. Peng, K.K. Huang, Z. Shi, R.G. Xie, W.S. Yang, Nano Res. 9 (2016) 1994–2006.
[22] A. Swarnkar, R. Chulliyil, V.K. Ravi, M. Irfanullah, A. Chowdhury, A. Nag, Angew. Chem. Int. Ed. 54 (2015) 15424–15428.
[23] K. Nikolaidou, S. Sarang, C. Hoffman, B. Mendewala, H. Ishihara, J.Q. Lu, B. Ilan, V. Tung, S. Ghosh, Adv. Opt. Mater. 4 (2016) 2126–2132.
[24] S. Mirershadi, S. Ahmadi-Kandjani, Dyes Pigments 120 (2015) 15–21.
[25] H. Zhu, Y. Fu, F. Meng, X. Wu, Z. Gong, Q. Ding, M.V. Gustafsson, M.T. Trinh, S. Jin, X.Y. Zhu, Nat. Mater. 14 (2015) 636–642.
[26] F. Meinardi, S. Ehrenberg, L. Dhamo, F. Carulli, M. Mauri, F. Bruni, R. Simonutti, U. Kortshagen, S. Brovelli, Nat. Photon. 11 (2017) 177–185.
[27] L.H. Slooff, E.E. Bende, A.R. Burgers, T. Budel, M. Pravettoni, R.P. Kenny, E.D. Dunlop, A. Büchtemann, Phys. Status Solidi – Rapid Res. Lett. 2 (2008) 257–259.
[28] C. Yang, R.R. Lunt, Adv. Opt. Mater. 5 (2017) 1600851.
[29] A. Goetzberger, W. Greube, Appl. Phys. 14 (1977) 123–139.
[30] X. Wang, G.I. Koleilat, J. Tang, H. Liu, I.J. Kramer, R. Debnath, L. Brzozowski, D.A.R. Barkhouse, L. Levina, S. Hoogland, E.H. Sargent, Nat. Photonics 5 (2011) 480–484.
[31] K. Wu, H. Li, V.I. Klimov, Nat. Photonics 12 (2018) 105–110.
[32] S. Zhu, Q. Meng, L. Wang, J. Zhang, Y. Song, H. Jin, K. Zhang, H. Sun, H. Wang, B. Yang, Angew. Chem. Int. Ed. 52 (2013) 3953–3957.
[33] Y. Liu, L. Zhou, Y. Li, R. Deng, H. Zhang, Nanoscale 9 (2017) 491–496.
[34] R.K. Das, S. Mohapatra, J. Mater. Chem. B 5 (2017) 2190–2197.
[35] J.C. Goldschmidt, M. Peters, A. Bösch, H. Helmers, F. Dimroth, S.W. Glunz, G. Willeke, Sol. Energy Mater. Sol. Cells 93 (2009) 176–182.
[36] S.J. Yoon, S. Draguta, J.S. Manser, O. Sharia, W.F. Schneider, M. Kuno, P.V. Kamat, ACS Energy Lett. 1 (2016) 290–296.
[37] F. Liu, Y. Zhang, C. Ding, S. Kobayashi, T. Izuishi, N. Nakazawa, T. Toyoda, T. Ohta, S. Hayase, T. Minemoto, K. Yoshino, S. Dai, Q. Shen, ACS Nano 11 (2017) 10373–10383.
[38] B.A. Koscher, J.K. Swabeck, N.D. Bronstein, A.P. Alivisatos, J. Am. Chem. Soc. 139 (2017) 6566–6569.
[39] Z. Wang, F. Yuan, X. Li, Y. Li, H. Zhong, L. Fan, S. Yang, Adv. Mater. 29 (2017) 1702910.
[40] Y. Zhang, X. Liu, Y. Fan, X. Guo, L. Zhou, Y. Lv, J. Lin, Nanoscale 8 (2016) 15281–15287.
[41] V.I. Klimov, T.A. Baker, J. Lim, K.A. Velizhanin, H. McDaniel, ACS Photonics 3 (2016) 1138–1148.

Haiguang Zhao is Professor of College of Physics & The State Key Laboratory, Qingdao University, Qingdao (Shandong), China. He received M.Sc. degree (2007) from Zhejiang University and Ph.D. degree (2012) from Institut National de la Recherche Scientifique (INRS), Quebec University. His research interests focus on the synthesis of low-dimensional semiconductor materials (including metal oxide, quantum dot, nanoplatelets and inorganic perovskite) for solar energy applications, such as solar cell, luminescent solar concentrator and solar-driven water splitting.

Daniele Benetti received his B.Sc. and M.Sc. degrees in Electronic Engineering from University of Brescia (Italy). He is currently pursuing his Ph.D. in material science under the supervision of Prof. Federico Rosei at the Institut National de la Recherche Scientifique (INRS, Canada). His recent research focuses on the investigation of electronic and ionic processes of excitonic solar cells and the development of large area Luminescent Solar Concentrators (LSCs) based on quantum dots.

Xin Tong obtained his bachelor's degree from School of Microelectronics and Solid-State Electronics, University of Electronic Science and Technology of China (UESTC) in 2014. He is currently a joint Ph.D. student in Institute of Fundamental and Frontier Sciences, UESTC and Institut National de la Recherche Scientifique (INRS, Canada). His research interests focus on the design and synthesis of colloidal quantum dots and their further applications in solar technology such as photoelectrochemical (PEC) cells for hydrogen generation and solar cells.

Hui Zhang obtained his Bachelor's degree in Materials Physics and Master's degree in Materials Engineering from Sichuan University, China, in June 2012 and June 2015, respectively. During his Master study, his research focused on nanocomposite materials and their applications in electrochemistry. He is currently a Ph.D. student under the joint supervision of Prof. Federico Rosei and Prof. Shuhui Sun at INRS-EMT supported by MATECSS Excellence Scholarship, conducting research on design and synthesis of quantum dots for solar technologies.

Yufeng Zhou received a Master Degree at University of Science and Technology of China (2013). She continued her research work in Chengdu Green Energy and Green Manufacturing Technology R&D Center in China as a research assistant for one year. She is currently a Ph.D. student at the Institut National de la Recherche Scientifique (INRS, Canada) with Materials and Technologies for Energy Conversion, Saving and Storage (MATECSS) excellence scholarship. Her research mainly focuses on the synthesis of semiconducting nanomaterials (such as colloidal quantum dots and nanoplatelets) and their applications in luminescent solar concentrators and solar-driven water splitting.

Guiju Liu received her Bachelor degree in Materials Physics from Qingdao University (China) in 2014. She obtained Master degree at Qingdao University (China) in 2017. Currently, she is a Ph.D. student majoring in Materials Physics and Chemistry at Qingdao University. Her research mainly focuses on the synthesis and structural characterization of quantum dots and their applications in luminescent solar concentrators and hydrogen generation.

Dongling Ma is currently a full professor at INRS. Her main research interest consists in the development of various nanomaterials (e.g., quantum dots, catalytic nanoparticles, plasmonic nanostructures, and different types of nanohybrids) for applications in energy (e.g., solar cells), catalysis (including photocatalysis) and biomedical sectors. Before joining INRS in July 2006, she was awarded Natural Sciences and Engineering Research Council Visiting Fellowships and worked at National Research Council of Canada from 2004–2006. She received her Ph.D. degree from Rensselaer Polytechnic Institute (USA) in 2004.

Shuhui Sun directs the Laboratory of Sustainable Nanotechnology (SUN) at INRS, center for Energy, Materials, and Telecommunications, Canada. Prof. Sun's current research interests focus on the development of multifunctional nanomaterials for Energy and Environment, including PEM fuel cells (low-Pt and Pt-free catalysts), Li-ion and Na-ion batteries, metal–air batteries, as well as Water treatment. His several recent awards include the member of Global Young Academy (2017), ECS-Toyota Young Investigator Fellow (2017), IUPAC Novel Materials Youth Prize (2017).

Zhiming M. Wang received his B.S. degree in applied physics from Qingdao University, Qingdao, China, in 1992, his M.S. degree in physics from Peking University in Beijing, China, in 1995, and his Ph.D. degree in condensed matter physics from the Institute of Semiconductors at the Chinese Academy of Sciences in Beijing, China, in 1998. He is currently a Professor of National 1000-Talent Program, working in the University of Electronic Science and Technology of China. His research interests include the optoelectronic properties of low-dimensional semiconductor nanostructures and corresponding applications in photovoltaic devices.

Yiqian Wang received his Ph.D. degree in condensed matter physics from Institute of Physics, Chinese Academy of Sciences, China in 2001. Then he worked as a research fellow at INRS-EMT, Canada and Imperial College London, UK. He is currently a Professor at Qingdao University. His research interest includes the fabrication and characterization of perovskite functional materials, as well as exploitation of their potential applications.

Federico Rosei is Professor and Director of the INRS Centre Énergie, Matériaux et Télécommunications, Varennes (QC) Canada. He holds the UNESCO Chair in Materials and Technologies for Energy Conversion, Saving and Storage and the Senior Canada Research Chair in Nanostructured Materials. He received M.Sc and Ph.D. degrees from the University of Rome “La Sapienza” in 1996 and 2001, respectively. He has received several awards and is Fellow/Member of many prestigious societies and academies, including the Royal Society of Canada, the European Academy of Sciences, the American Physical Society, the World Academy of Arts and Science, the Chinese Chemical Society (Honorary), the American Association for the Advancement of Science, SPIE, the Canadian Academy of Engineering, ASM International and the Engineering Institute of Canada.